Carbon-13 Relaxation in Paramagnetic Complexes of Amino Acids. Structural and Dynamical Information on a Manganese(II) Complex of Histidine

Jens J. Led*[1a] and David M. Grant[1b]

Contribution from the Chemical Laboratory V, The H.C. Ørsted Institute, University of Copenhagen, 2100 Copenhagen, Denmark, and the Department of Chemistry, University of Utah, Salt Lake City, Utah 84112. *Received February 10, 1975*

Abstract: The carbon-13 relaxation (T_1 and T_2) and the carbon-13 isotropic contact shift of histidine in aqueous solution at pH 10.5, caused by the presence of Mn^{2+} ions in low concentrations, have been measured. For all six histidine carbons the T_1 relaxation times were measured at least at two temperatures (310 and 343 K) while the temperature variation of the T_2 relaxation times of the same atoms, as well as the isotropic contact shift for five of the histidine carbons and the water protons, were measured over a temperature range of 70–80° C. From these results the number of histidine molecules in the coordination sphere of the metal ions and the coupling constants for the hyperfine interaction between the unpaired electrons and the individual carbon-13 nuclei in these molecules have been evaluated, as well as the kinetic parameters for the exchange of the histidine ligands between the coordination sphere and the bulk histidine solution. Furthermore, it is found that the experimental results can be interpreted in terms of the model of Bloembergen and Morgan, according to which the electronic relaxation is caused by collision modulation of a transient zero field splitting (ZFS) interaction. Thus, the experimental results have yielded information about the ZFS interaction and the electronic relaxation and its temperature dependence. Likewise, estimated values of the correlation time for the molecular diffusional rotation and its activation energy have been obtained. Based on these results it has been concluded, that while the spin–lattice relaxation of the carbon-13 nuclei caused by the unpaired electrons is due to the dipolar interaction only, the paramagnetic contribution to the carbon-13 spin–spin relaxation is primarily controlled by scalar interaction. Finally, it is found that the distances between the Mn^{2+} ion and the individual carbon atoms in the ligand evaluated from the dipolar relaxation terms are in agreement with an octahedrally coordinated Mn^{2+} complex and correspond, with a single exception, closely to the distances expected from the crystal structure of the bis(histidino)-nickel(II) complex. The experimental accuracy of the structural parameters obtained by this method for a metal complex in solution is found to be comparable to the accuracy of X-ray structures of similar compounds in the crystal phase.

I. Introduction

NMR studies of paramagnetic metal complexes have provided an important method for elucidating the structure of these systems in solution as interatomic distances between protons and paramagnetic transition metal ions may be determined from the unpaired electron contribution to the relaxation times of the protons.[2,3] Recently, also Mn^{2+}–^{13}C distances have been estimated from such relaxation data.[4,5] In general results of this type have been in agreement with distances obtained by X-ray crystallography when a comparison has been possible. Likewise, structural information has been obtained from changes in chemical shifts caused by paramagnetic ions of the lanthanide series.[6,7] While a structural interpretation of the data obtained by this latter method is not always possible because of complexities in the interaction, the first approach is in principle straightforward due to the simple relation usually existing between the paramagnetic contribution to the relaxation rates of a nucleus and its distance from the paramagnetic ion.

This method has, however, certain inherent limitations when the magnetic nuclei are protons. First, the relatively narrow range of chemical shielding for protons may combine with the broad lines often found in paramagnetic species to give seriously overlapping proton lines. This situation may prevent one from extracting the separate relaxation parameters for individual proton transitions especially when large molecules are studied. Second, protons generally are strongly spin coupled to other magnetic nuclei in the molecule, especially other protons, through the hyperfine interaction and this may unduly complicate the extraction of parameters. Third, protons are often at the periphery in most complexes leading to proton metal distances which are relatively long compared with the corresponding distances between the metal ion and the heavier atoms of the ligand such as C, N, or O. This tends to decrease the contribution of the paramagnetic ion to the relaxation and amplifies the inaccuracies arising from paramagnetic ions in neighboring molecules, particularly when dealing with small ligand molecules and high concentrations of the paramagnetic ions. These difficulties have restricted the application of the method as far as protons are concerned[2,3] mainly to water molecules directly attached to a paramagnetic ion or to groups of equivalent protons in rather large biomolecules. Finally, in most cases only upper limits of the nuclei–metal distances have been estimated because information on the effect of chemical exchange on the relaxation process is often lacking.

If ^{13}C nuclei, either in natural abundance or in specifically labeled molecules, are studied, these disadvantages can be eliminated or significantly reduced. Here, the greater chemical shift range for ^{13}C tends to eliminate overlapping lines. Furthermore, proton decoupling usually collapses spin–spin multiplets to singlets leaving the relaxation of the ^{13}C nuclei governed by a single exponential time constant,[8] and ^{13}C nuclei are generally closer to the paramagnetic center and therefore not affected as greatly by intermolecular interactions. Despite these advantages of ^{13}C it is still necessary to unravel the relative importance of the different competing mechanisms of relaxation for the observed nuclei in order to obtain the metal–carbon distances from the experimental relaxation data. To do this one has to determine the relaxation of the paramagnetic electrons and the hyperfine coupling between these and the observed ^{13}C nuclei as well as the kinetics of the ligand exchange process. This paper presents such a ^{13}C investigation of a Mn^{2+} complex in aqueous solution. Histidine was chosen as the ligand, because this amino acid frequently constitutes the binding site for metal ions in many biological molecules.[9] Fortunately,

the X-ray structures of complexes of this amino acid with several bivalent metal ions are well known[10] and these data may be used to give confidence in the method. In Figure 1 is shown, schematically, the octahedral structure found for these complexes in the cases of Co^{2+} and Ni^{2+}.[10] Manganese(II) forms complexes with histidine in water solution[11,12] as well as with the histidine residue in larger biological systems,[2a,13] although no structural parameters revealing the specific arrangement of the carbon framework of the ligand amino acid relative to the Mn^{2+} ion has been reported for these complexes neither in the liquid nor in the crystalline phase. Furthermore the Mn^{2+} ion is known to exhibit a nearly isotropic g tensor[14] and relative long relaxation times[15-18] for its unpaired electrons. Both of these features simplify the interpretation of the relaxation data and thereby improve the possibility of obtaining structural information.

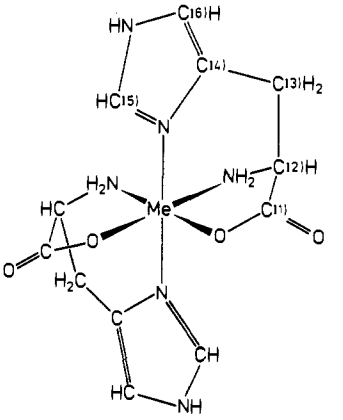

Figure 1. Schematic structure of an octahedral histidine-Me^{2+} complex.

II. Theory

A. The Influence of Paramagnetic Ions on the Nuclear Relaxation. When coupling between the electron orbital and spin-angular momenta can be neglected, which is generally the case for ions in the first transition series,[19] the paramagnetic contribution to the relaxation rate of an adjacent nuclear spin is given by the combined Solomon-Bloembergen equations.[20-23] For Mn^{2+} complexes, the experimentally found values for the electron relaxation time, T_e, are in the range 10^{-8}–10^{-9} sec at room temperature[15-18] while the correlation time for the molecular rotational reorientation, τ_R, at the same temperature is approximately 10^{-10}–10^{-11} sec for molecules of the size of a histidine–manganese complex in solutions of low viscosity. Therefore, under these conditions $1/T_e \ll 1/\tau_R$. Furthermore, in most Mn^{2+} complexes of the type considered here, it is observed[14,24,25] that $1/\tau_M \lesssim 1/T_{1e}$ at room temperature or slightly above this temperature. Here τ_M is the mean residence time of the nucleus in the first coordination sphere of the complex, and characterizes the rate of ligand exchange. For these inequalities the correlation time for the electron–^{13}C dipolar interaction, τ_c, will be equal to τ_R. When using this effective correlation time in combination with the ratio $\omega_S/\omega_I \sim 2600$ between the Lamor frequencies ω_S and ω_I of the electron and the ^{13}C nucleus, respectively, as well as the following inequalities that all apply at the magnetic field strength used in this work; $\omega_I^2\tau_R^2 \ll 1$, $\omega_S^2\tau_R^2 > 1$, and $\omega_S^2\tau_{e,l}^2 \gg 1$, where $\tau_{e,l}$ is the correlation time for the scalar interaction, the Solomon–Bloembergen equations reduce to:

$$\frac{1}{T_{1M}} = \frac{2}{5}\frac{S(S+1)g^2\beta^2\gamma_I^2}{r^6}\tau_R \qquad (1)$$

$$\frac{1}{T_{2M}} = \frac{7}{15}\frac{S(S+1)g^2\beta^2\gamma_I^2}{r^6}\tau_R + \frac{1}{3}\frac{S(S+1)A^2}{\hbar^2}\tau_{e,I} \qquad (2)$$

where S is the electron spin of the paramagnetic ion, while γ_I is the gyromagnetic ratio of the observed nucleus and g and β are the g value for the paramagnetic electrons and the Bohr magneton, respectively; r is the distance between the paramagnetic center and the observed nucleus in the bound ligand. A is the hyperfine coupling constant between the paramagnetic electrons and the observed nuclei, while $\tau_{e,I}$ is given by:

$$\frac{1}{\tau_{e,I}} = \frac{1}{T_{1e}} + \frac{1}{\tau_M} \qquad (3)$$

As it appears from eq 1 and 2 the scalar relaxation term contributes only in $1/T_{2M}$. This implies that the order of magnitude for the scalar coupling constant A is not significantly larger than the order of magnitude (10^6 Hz) found for similar couplings to protons.[17,26] Recently reported Mn^{2+}–^{13}C coupling constants are in agreement with this assumption.[5] Since the dipolar terms appear in both expressions with comparable coefficients (2/5 vs. 7/15), the relative significance of the dipolar and scalar relaxation mechanisms will be given by the relative magnitudes of $1/T_{1M}$ and $1/T_{2M}$. The scalar term in eq 2 is proportional to $\tau_{e,I}$ which, according to eq 3, depends upon T_{1e}. It has been shown[26,27] that this relaxation in diluted aqueous solution of the paramagnetic ions is controlled by modulation of the quadratic zero field splitting (ZFS) interaction. Thus, for an aqueous Mn^{2+} complex it is to a good approximation given[26,27] by:

$$\frac{1}{T_{1e}} = \frac{1}{25}\Delta^2[4S(S+1) - 3] \times \left[\frac{\tau_v}{1+\omega_S^2\tau_v^2} + \frac{4\tau_v}{1+4\omega_S^2\tau_v^2}\right] \qquad (4)$$

Here Δ is the ZFS parameter and τ_v is a time constant characteristic for the modulation of the ZFS interaction. For the Mn^{2+}-hexaaquo complex where the Mn^{2+} ions are in an isotropic environment, it has been found[27] that the ZFS interaction as well as its time modulation result from collisions between the complex and the bulk solvent molecules. If the paramagnetic ions are in an asymmetric environment there will, in addition, be a static ZFS interaction. The modulation of this by the rotational diffusion of the complex may also provide fluctuating fields for the electron relaxation.[28] The temperature dependence of τ_v and τ_R can be approximated[26] by the Arrhenius expression:

$$\tau_I = \tau_I^0 \exp(E_I/RT) \qquad (5)$$

while τ_M usually is given by the more elaborate Eyring expression:[29]

$$\frac{1}{\tau_M} = \frac{kT}{h}\exp\left[-\frac{\Delta H^\ddagger}{RT} + \frac{\Delta S^\ddagger}{R}\right] \qquad (6)$$

B. The Influence of Exchange Rate on Nuclear Relaxation. In order to observe the signal from the nuclei in the ligand, it becomes necessary, in most instances, to observe the resonance signal on a solution with a low concentration of the paramagnetic ion relative to the ligand to avoid inordinate line broadening. In addition, a temperature must be selected to give a ligand exchange rate between the coordination sphere and the bulk solution which is sufficiently fast on the NMR time scale to average the spectral features of the complex in with those of the unbound ligand. Under these conditions, the following expressions[30,31] are appropriate for relating T_{1M}, T_{2M}, τ_M, $\Delta\omega_M$, and pq to the ex-

perimental observables:

$$\frac{1}{T_{1,\text{obsd}}} - \frac{1}{T_1{}^0} = \frac{1}{T_{1P}} = \frac{1}{T_{1A'}} + \frac{pq}{T_{1M} + \tau_M} \quad (7)$$

$$\frac{1}{T_{2,\text{obsd}}} - \frac{1}{T_2{}^0} = \frac{1}{T_{2P}} = \frac{1}{T_{2A'}} + \frac{pq}{\tau_M}\left[\frac{(1/T_{2M} + 1/\tau_M)(1/T_{2M}) + \Delta\omega_M{}^2}{(1/T_{2M} + 1/\tau_M)^2 + \Delta\omega_M{}^2}\right] \quad (8)$$

where τ_M, T_{1M}, and T_{2M} have the same definition as above, $\Delta\omega_M$ is the contact shift, p is the ratio of metal to ligand concentration, and q is the number of coordinated ligands per metal ion. $1/T_1{}^0$ and $1/T_2{}^0$ are the relaxation rate of the nuclei in the free ligand while the adjusted relaxation rates $1/T_{1P}$ and $1/T_{2P}$ measure the paramagnetic contribution to the observed averaged relaxation rates $1/T_{1,\text{obsd}}$ and $1/T_{2,\text{obsd}}$. $1/T_{1A}'$ and $1/T_{2A}'$ are the contributions to the relaxation of the nuclei outside the first coordination sphere due to dipole-dipole interaction with the paramagnetic electrons. For protons[30] this contribution has been found to be less than 10% of $1/T_{1,\text{obsd}}$, while it is a significantly smaller fraction of $1/T_{2,\text{obsd}}$ when $1/T_{2M}$ is dominated by scalar relaxation. For reasons explained in section I these contributions are expected to be an even smaller fraction of $1/T_{1,\text{obsd}}$ and $1/T_{2,\text{obsd}}$ when ^{13}C is the observed nuclei and they are therefore neglected in this work. Assuming a Curie law temperature dependence and an isotropic g value for the system, the isotropic contact shift, $\Delta\omega_M$, between the bound nuclei and the unbound nuclei has been given[32,33] by:

$$\frac{\Delta\omega_M}{\omega_I} = \frac{\Delta H}{H} = -\frac{g\beta S(S+1)}{3\hbar\gamma_N kT} A \quad (9)$$

where the symbols have their usual meaning. In case of chemical exchange, the experimental frequency shift is given[31] by:

$$\Delta\omega_P = \frac{pq}{\tau_M{}^2}\left[\frac{\Delta\omega_M}{(1/T_{2M} + 1/\tau_M)^2 + \Delta\omega_M{}^2}\right] \quad (10)$$

for the same approximation as used in eq. 7 and 8.

III. Experimental Section

Highly purified L-histidine (free base) and analytical reagent $MnCl_2 \cdot 4H_2O$ were used. The manganese salt was dried in vacuo at 220°C until the waters of crystallization were excluded. All samples were 1.90 M solutions of histidine in distilled, deionized water at pH 10.5, and with a concentration of Mn^{2+} ranging from 0 to 0.01 M. In the samples used for measuring the isotropic contact shift of the water protons, 93% of the H_2O was replaced by D_2O. All samples were prepared in a nitrogen atmosphere using water which had been purged with nitrogen for 30 min. The solutions were then sealed off in vacuo. Samples prepared in this manner exhibited no precipitation of the $Mn(OH)_2$. Neither did the samples or the spectra change during the period of the study.

High resolution ^1H noise-decoupled ^{13}C NMR spectra were obtained at 25.2 MHz using a Varian XL100-15 spectrometer equipped with Fourier pulse gear and a 620f computer. Typical overall plots of the ^{13}C spectrum of histidine are shown in Figure 2. With the probe (V4415) and rf power used in the T_1 experiments the width of the 90° pulse was 100 μsec for a carrier frequency which differs 500 Hz from the resonance line, while in the line width and contact shift measurements (probe V4412) the 90° pulse was 16 μsec, practically independent of the distance from the carrier frequency within the frequency range of the spectrum. The 100 MHz proton-decoupling field was produced by a Hewlett-Packard 510A frequency synthesizer combined with a Hewlett-Packard 5110B frequency synthesizer driver and amplified with a 10 W ENI Model 310L wide-band rf amplifier connected with a 100 MHz filter. All proton spectra were continuous wave spectra obtained at 90 MHz using a Bruker HX 90 spectrometer equipped with a deuterium lock. During all experiments, the temperature was kept constant within ±1°C. In order to eliminate the shift arising from the change in the bulk susceptibility caused by the paramagnetic metal ions *p*-dioxane was used as an internal standard in all experiments because of the unlikelihood of its competition with histidine and water in entering the first coordination sphere of the metal ion.

The T_1 relaxation times were measured from partial, relaxed Fourier transform spectra employing a 90°-$4T_1$-180°-τ-90° pulse sequence. The time between sequences was equal or greater than $4T_1$'s. Since the applied pulse rf field H_1 is equivalent only to 2500 Hz, the residual static magnetic field h_0 in the rotating frame corresponding to the off-resonance position of the carrier frequency is not negligible, which makes $H_{1,\text{eff}}$ slightly unequal to H_1. For a given position of the carrier frequency $H_{1,\text{eff}}$ and thereby the times necessary for the 180 and 90° pulses will therefore be different for the individual carbon signals in the spectrum. In order to eliminate errors in the T_1 values caused by this variation in $H_{1,\text{eff}}$, the measurements were made separately for each carbon with a 500 Hz off-resonance position of the carrier frequency and pulse widths calibrated for this offset. T_2 values were determined assuming a Lorentzian line shape and the relation $\Delta\nu_{1/2} = 1/\pi T_2$. A delay of $4T_1$ was applied between 90° pulses to ascertain the validity of this equation.[34] In order to minimize errors due to differences in temperature and inhomogeneity broadening, corresponding values of $T_{2,\text{obsd}}$ and $T_2{}^0$ as well as $T_{1,\text{obsd}}$ and $T_1{}^0$ were measured sequentially as pairs. The isotropic contact shifts for the ^{13}C nuclei were obtained from spectra used in the $T_{2,\text{obsd}}$ measurements.

Due to the broad water proton signal in the paramagnetic samples it was difficult to measure the frequency shift, $\Delta\omega_p$, of this line, directly. Instead it was obtained as the negative value of the frequency shift of the sharp, well-defined proton signal from the internal dioxane standard, that was observed when the signal from the internal D_2O was used as a lock. With this lock the addition of the paramagnetic ions changes the magnetic field by an amount corresponding to the sum of the bulk susceptibility shift and the isotropic contact shift of the D_2O signal. This leaves the chemical shift of the H_2O signal unchanged relative to the lock when comparing samples with and without paramagnetic ions, while the proton signal from the internal dioxane, which is only affected by the change in the bulk susceptibility, will be shifted by an amount corresponding to the isotropic contact shift of the H_2O signal (and D_2O signal in ppm) but in the opposite direction. Contrary to the H_2O signal the D_2O line is sufficiently narrow at the paramagnetic ion concentration (0.01 M Mn^{2+}) used here to constitute a well-defined lock signal. This difference in the relative broadening of the two signals is, of course, due to the A^2 dependence of $1/T_{2M}$.

The static magnetic susceptibility was measured using the NMR method described by Evans[35] and Deutsch et al.[36] The samples were sealed, deoxygenated histidine solutions identical with those used in the ^{13}C relaxation and contact shift experiments, except for a higher concentration of paramagnetic ions in the paramagnetic sample. The susceptibility shift resulting from the presence of the paramagnetic ions were measured as the change in chemical shift of the ^{13}C line of the internal dioxane reference, relative to the D_2O lock signal as external reference. The D_2O used for lock was placed in the annulus between a 12 mm tube and a 10 mm tube containing the sample.

IV. Results and Discussion

A. Magnetic Susceptibility. The paramagnetic susceptibility shift of the ^{13}C line from the internal *p*-dioxane reference was measured at three different temperatures. As shown in Figure 3, the shift is inversely proportional to the absolute temperature in agreement with Curie's law. The average value of the shift at 70°C is 30 ± 2 Hz. This corresponds closely with the expected shift[35,36] of 31.2 Hz for a 0.047 M solution of a "spin-only" paramagnetic ion with $S = 5/2$, in agreement with octahedrally coordinated, high-spin Mn^{2+} ions over the entire observed temperature range. Consequently, an electronic magnetic moment, $\mu = g\beta[S(S+1)]^{1/2}$, corresponding to $S = 5/2$, was used throughout this work.

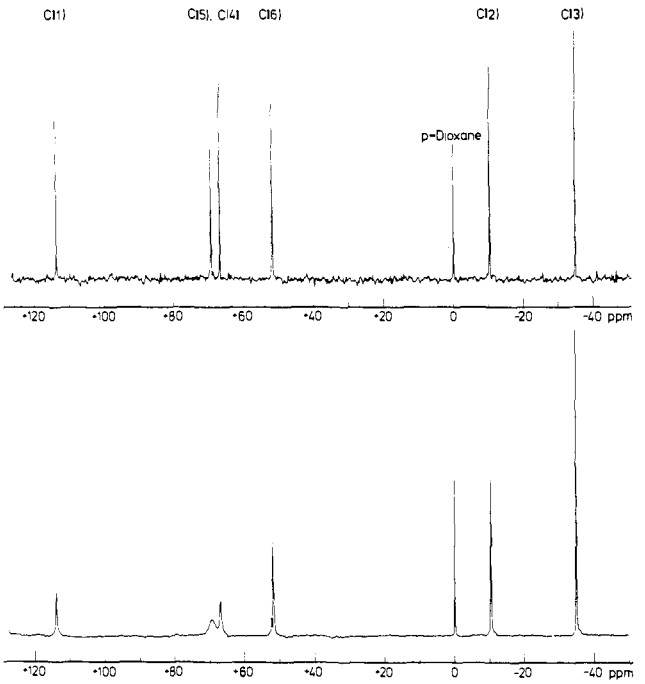

Figure 2. Carbon-13 spectra at 23.5 kG of 1.90 *M* solutions of histidine in water at pH 10.5 and 353 K, with *p*-dioxane as internal standard. The solution corresponding to the lower spectrum contains, in addition, 5.00×10^{-4} *M* $MnCl_2$. The spectra demonstrate the different effects on the individual signals when the paramagnetic Mn^{2+} ions are added.

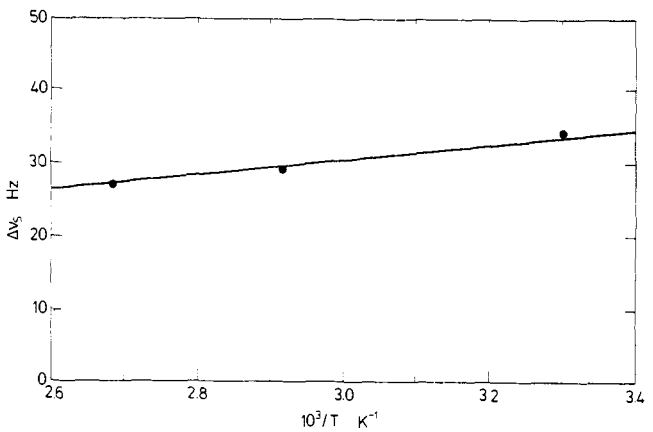

Figure 3. Temperature variation of the paramagnetic susceptibility shift of the ^{13}C signal of *p*-dioxane, for $[Mn^{2+}] = 0.047$ *M* and a magnetic field of 23.5 kG. The shift was measured as described in the text.

B. Relaxation and Isotropic Contact Shift Data. Each T_1 value was extracted from 10–12 partially relaxed Fourier transform spectra by a two-parameter (T_1 and $S(\infty)$) least-squares fit of eq 11. This exponential equation was fitted directly to the experimental data,

$$y = S(\infty) - S(t) = 2S(\infty) \exp\left(-\frac{\tau}{T_1}\right) \qquad (11)$$

in order to ascertain an equal weighting of the data points. In this way $1/T_1^0$ and $1/T_{1,obsd}$ were obtained for all six carbon atoms in the ligand at 310 and 343 K and the results are given in Table I together with the calculated values for $1/T_{1P}$. Due to extensive broadening of the signals from C(4) and C(5) at the Mn^{2+} concentration typically used here (5.00×10^{-4} *M*), the $1/T_{1P}$ values for these two carbons were obtained from a solution with a 5 times lower Mn^{2+} concentration. To check the reliability of the final

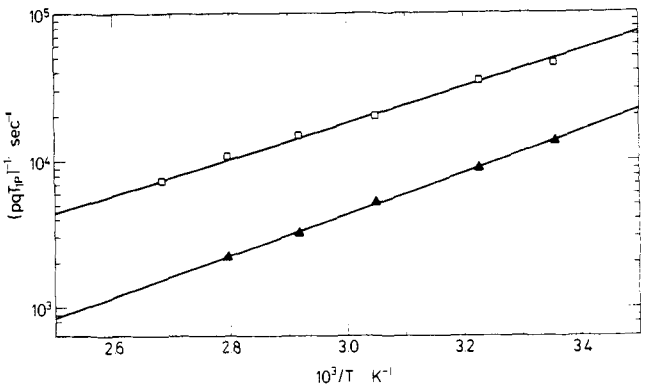

Figure 4. Temperature variation of the normalized experimental T_{1P}^{-1} relaxation rates for histidine carbons, obtained at 23.5 kG from a 1.90 *M* solution of histidine in water at pH 10.5 and with $[Mn^{2+}] = 5.00 \times 10^{-14}$ *M*: (□) C(2), (▲) C(6). The curves were computed using the activation energies, E_R, in Table II and correspond to the best fit.

Table I. Experimental ^{13}C Spin–Lattice Relaxation Rates for the Histidine Carbons Including 2σ Confidence Limits

	$1/T_{1,obsd}$, sec^{-1}	$1/T_1^0$, sec^{-1}	$1/T_{1P}$, sec^{-1}	$1/T_{1P}$ (normalized[c]), sec^{-1}
		310 K		
C(1)	1.90 ± 0.09[b]	0.14 ± 0.02	1.76 ± 0.09	8.80 ± 0.48
C(2)	11.75 ± 1.00[a]	1.14 ± 0.04	10.61 ± 1.00	10.61 ± 1.00
C(2)	3.17 ± 0.19[b]	1.14 ± 0.04	2.03 ± 0.20	10.15 ± 1.00
C(3)	5.65 ± 0.25[a]	2.01 ± 0.07	3.64 ± 0.26	3.64 ± 0.26
C(4)	1.43 ± 0.11[b]	0.18 ± 0.02	1.25 ± 0.11	6.25 ± 0.55
C(5)	2.27 ± 0.22[b]	1.13 ± 0.04	1.14 ± 0.22	5.70 ± 1.10
C(6)	3.79 ± 0.37[a]	0.99 ± 0.04	2.80 ± 0.38	2.80 ± 0.38
C(6)	1.55 ± 0.05[b]	0.99 ± 0.04	0.56 ± 0.06	2.80 ± 0.30
		343 K		
C(1)	3.66 ± 0.21[a]	0.039 ± 0.006	3.62 ± 0.21	3.62 ± 0.21
C(2)	4.95 ± 0.32[a]	0.47 ± 0.02	4.48 ± 0.32	4.48 ± 0.32
C(2)	1.32 ± 0.07[b]	0.47 ± 0.02	0.85 ± 0.07	4.25 ± 0.35
C(3)	2.46 ± 0.08[a]	0.78 ± 0.03	1.68 ± 0.09	1.68 ± 0.09
C(4)	0.56 ± 0.05[b]	0.05 ± 0.005	0.51 ± 0.05	2.55 ± 0.25
C(5)	0.90 ± 0.09[b]	0.46 ± 0.02	0.44 ± 0.09	2.20 ± 0.45
C(6)	1.40 ± 0.09[a]	0.40 ± 0.02	1.00 ± 0.09	1.00 ± 0.09
C(6)	0.62 ± 0.03[b]	0.40 ± 0.02	0.22 ± 0.04	1.10 ± 0.18

[a] $[Mn^{2+}] = 5.00 \times 10^{-4}$ *M*. [b] $[Mn^{2+}] = 1.00 \times 10^{-4}$ *M*. [c] Data normalized to $[Mn^{2+}] = 5.00 \times 10^{-4}$ *M*.

normalization shown in Table I, the $1/T_{1P}$ values of C(2) and C(6) were measured at both concentrations. For these two carbons the temperature variation of $1/T_{1P}$ over a temperature range of 80 K, as shown in Figure 4, was also determined. Likewise, the temperature dependence of $1/T_{2P}$ for all six carbons was measured over the same temperature range and these results are given in Figure 5. Finally the temperature variations of the experimental shifts $\Delta\nu_P$, caused by the hyperfine contact interaction, were obtained for the same atoms except C(2), since the shift for this carbon was of the same magnitude as the uncertainty in the measurements (ca. ±0.5 Hz). These results are shown in Figure 6.

C. The Dominant Mechanisms of Relaxation. In order to establish the relative importance of the different mechanisms which according to section II can influence the relaxation of the ^{13}C nuclei in the histidine ligand, a least-squares fit of eq 2-10 was made to the $1/T_{2P}$ and $\Delta\nu_P$ data for all six carbons, simultaneously. In order to justify this procedure the reasonable assumption was made that the histidine molecules exchange as a whole in the exchange process in and out of the first coordination sphere of the Mn^{2+} ions. This assumption is strongly supported by the quality of the fit (see Figures 5 and 6). In the calculations

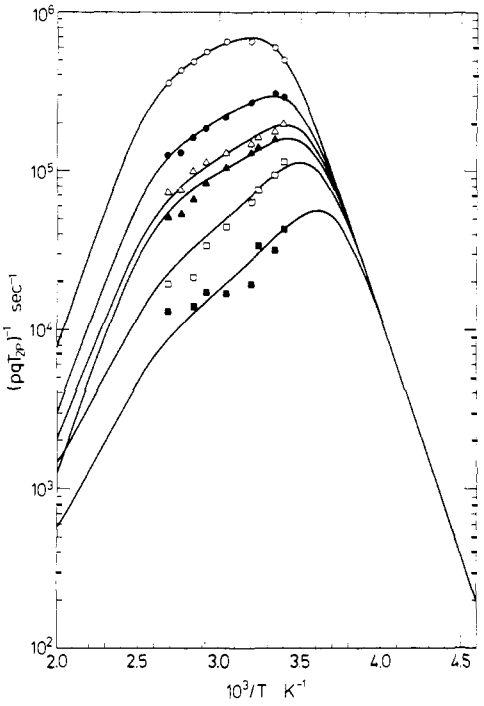

Figure 5. Temperature variation of the normalized experimental T_{2P}^{-1} relaxation rates for the histidine carbons, obtained at 23.5 kG from a 1.90 M solution of histidine in water at pH 10.5 and with $[Mn^{2+}]$ = 1.00×10^{-4}–5.00×10^{-4} M: (△) C(1), (□) C(2), (■) C(3), (●) C(4), (○) C(5), (▲) C(6). The curves were computed using the parameters in Table II and correspond to the best fit.

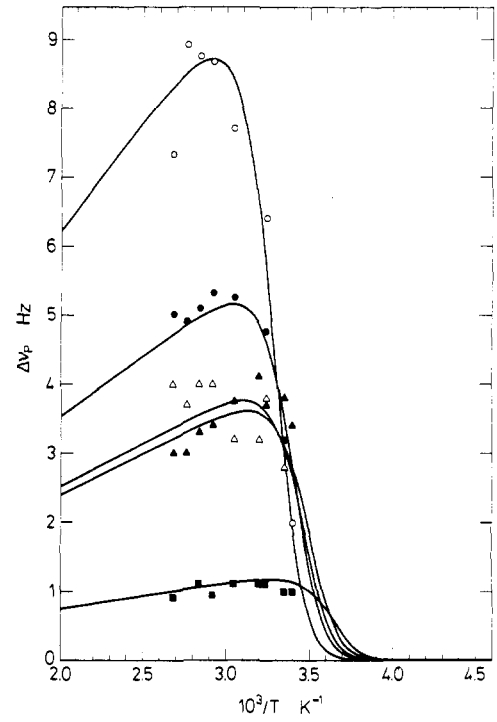

Figure 6. Temperature variation of the experimental contact shift, $\Delta\nu_P$, of the histidine carbons obtained at 23.5 kG from a 1.90 M solution of histidine in water at pH 10.5 and with $[Mn^{2+}] = 5.00 \times 10^{-4}$ M. All shifts are toward lower field and were measured relative to p-dioxane as internal standard: (△) C(1), (■) C(3), (●) C(4), (○) C(5), (▲) C(6). The curves were computed using the parameters in Table II and correspond to the best fit.

the dipolar terms in eq 2 were evaluated as $7/(6pq)$ times the corresponding $1/T_{1P}$ values. An activation energy of 6 kcal/mol (see below and Table II) was used for all six carbon atoms in calculating the temperature dependence of the correlation time τ_R for the diffusional rotation, given by eq 5. Since the experimental $1/T_{2P}$ and $\Delta\nu_P$ data presented here only allow a determination of 10 parameters out of the 12 parameters involved in the simultaneous fit, it was necessary to obtain two of the parameters from other sources. Furthermore, one of these parameters must be of the group $\Delta H^{\ddagger}$, $\Delta S^{\ddagger}$, τ_v^0, E_v, while the other one should be chosen among the rest of the parameters. In the present calculation a value of 3.9 kcal/mol[26] was assumed for E_v (to be discussed below) while pq was estimated via a determination of pq for the solvent water obtained from the experimental isotropic shift of the water proton signal (Figure 7) in the water histidine samples.

The mere fact that such a shift is observed in these samples shows qualitatively that the first coordination sphere of the manganese ions is still partly occupied by water molecules, despite the large surplus of histidine compared to Mn^{2+}. This is in contrast to what has been found[37] for an aqueous solution of histidine-containing Co^{2+} ions. Here, under conditions comparable to those used in the present study, the contact shift for the water protons was equal to zero, showing that histidine has replaced all water in the first coordination sphere of the Co^{2+} ions. This difference, however, is qualitatively in agreement with the observation of a smaller formation constant[38] for the Mn^{2+}–histidine complex than for the corresponding Co^{2+} complex.

The simple Curie law temperature dependence exhibited in the present study by the isotropic contact shift of the water protons is only compatible with eq 10 if $(\tau_M)^{-2} \gg (T_{2M})^{-2}$ and $(\Delta\omega_M)^{-2}$. In this case eq 10 can be reduced to:

$$\Delta\omega_P = pq\Delta\omega_M \qquad (12)$$

which, according to eq 9, has the Curie law temperature dependence. A quantitative determination of pq for the water ligand can therefore be made by fitting eq 12 to the experimental contact shift data if the electron–proton hyperfine coupling constant, $A(H_2O)$, is known. This can to a good approximation be obtained from the contact shift of the water protons in a similar solution of Mn^{2+} ions in water at the same pH as the histidine samples, but not containing this compound. Thus, a least-squares fit of eq 12 to the $\Delta\nu_P$ data for the protons in a pure water–Mn^{2+} sample presented in the upper part of Figure 7 gave for $p = [Mn^{2+}]/([H_2O] + [D_2O]) = (1.86 \pm 0.02) \times 10^{-4}$ and $q(H_2O) = 6$ a hyperfine coupling constant, $A(H_2O) = (7.68 \pm 0.44) \times 10^5$ Hz, a value somewhat larger than the value of 6.2×10^5 Hz reported by Luz and Shulman[17] but in good agreement with the value $(8.1 \pm 0.8) \times 10^5$ Hz reported by Hausser and Noack.[39] The uncertainty stated for the hyperfine coupling constant obtained in the present work as well as the error limits given in the following are the estimated 95% confidence limits. By using the value of the coupling constant found here a fit of eq 12 to the data in the lower part of Figure 7 gave $q = 2.40 \pm 0.16$ for $p = (2.06 \pm 0.02) \times 10^{-4}$; i.e., in the histidine–water mixture the first coordination sphere of the Mn^{2+} ions contains on an average 2.40 ± 0.16 water molecules ($D_2O + H_2O$). For a coordination number of 6 for the Mn^{2+} ions this leaves an average of $(6-2.4 \pm 0.16)/3 = 1.20 \pm 0.06$ tridentate histidine molecules in the first coordination sphere, corresponding to a mixture where ca. 20% of the Mn^{2+} ions have two histidine ligand while the remaining 80% have only one histidine and three water molecules as ligands. Consequently, one gets for $p = [Mn^{2+}]/[His] = (2.63 \pm 0.03) \times 10^{-4}$ that $pq = (3.16 \pm 0.15) \times 10^{-4}$.

The parameters obtained from the multiple regression analysis are shown in Table II together with the activation

Table II. Parameters Calculated from Experimental Relaxation and Contact Shift Data with 2σ Confidence Limits

(A/h)[C(1)], Hz	$(4.30 \pm 0.22) \times 10^5$	pq	$(3.16 \pm 0.15) \times 10^{-4}$	E_R[C(2)], kcal/mol	5.53 ± 0.40
(A/h)[C(2)], Hz	$(2.00 \pm 0.13) \times 10^5$	$\Delta H^{\ddagger}$, kcal/mol	13.26 ± 0.50	E_R[C(5)], kcal/mol	6.57 ± 0.20
(A/h)[C(3)], Hz	$(1.20 \pm 0.12) \times 10^5$	$\Delta S^{\ddagger}$, eu	13.8 ± 1.6	τ_M(298 K), sec	$(8.3 \pm 1.0) \times 10^{-7}$
(A/h)[C(4)], Hz	$(6.08 \pm 0.13) \times 10^5$	τ_v°, sec	$(8.4 \pm 1.3) \times 10^{-15}$	τ_v(298 K), sec	$(6.1 \pm 1.0) \times 10^{-12}$
(A/h)[C(5)], Hz	$(10.73 \pm 0.55) \times 10^5$	E_v, kcal/mol	3.9	T_{1e}(298 K), sec	$(7.6 \pm 0.7) \times 10^{-9}$
(A/h)[C(6)], Hz	$(4.12 \pm 0.55) \times 10^5$	ΔG	434 ± 34	τ_R(298 K),[b] sec	$(5.64 \pm 0.37) \times 10^{-10}$

[a] Reference 26. [b] See Section IVD.

energies for the rotational diffusion of the complex, extracted from the experimental T_{1P} data by a least-squares fit of eq 5. The $(pqT_{1P})^{-1}$, $(pqT_{2P})^{-1}$, and $\Delta\nu_P$ curves corresponding to these parameters are shown in Figures 4, 5, and 6. Table II also gives the values at 25°C of the three correlation times τ_M, τ_v, and T_{1e} calculated from the obtained parameters. Finally Table II contains an estimated value of the correlation time, τ_R, for the diffusional rotation of the complex obtained as described in section IVD.

All six electron–^{13}C hyperfine coupling constants correspond to isotropic contact shift toward lower field and are therefore positive. Those found for the carbons with π bonds are comparable in magnitude and sign to the above-mentioned electron–water proton coupling constants, while those corresponding to carbons with σ bonds only are somewhat smaller, indicating a relative lower delocalization of the paramagnetic electrons. All the measured electron–^{13}C coupling constants are of the same order of magnitude as similar hyperfine coupling constants found for the ^{13}C nuclei in the adenine ring of the Mn^{2+}-ATP complex[5] while they are numerically smaller than the electron–^{14}N coupling constants of 3.2×10^6 Hz found for the Mn^{2+}-acetonitrile complex[40] and the electron–^{17}O coupling constant of 2.7×10^6 Hz observed in the $Mn(H_2O)_6^{2+}$ complex.[31] These coupling constants were obtained from line width measurements only, which does not allow a determination of the signs. The values obtained for $\Delta H^{\ddagger}$ and τ_M(298 K) are comparable in magnitude to the $\Delta H^{\ddagger}$ and τ_M(298 K) values of ca. 14 kcal/mol and 1.1×10^{-6} sec found for the Mn^{2+}–AMP complex[41] and 11 kcal/mol and 6.5×10^{-6} sec found for the Mn^{2+}–ATP complex.[42]

Like the chosen value of E_v the calculated correlation time τ_v corresponds to a mechanism where the impact of the solvent molecules causes transient fluctuations in the symmetry of the complex, which provides fluctuating fields for the electron relaxation. Furthermore, the values obtained for τ_v and Δ are within the ranges of 3.3×10^{-12}–9.0×10^{-12} sec and 200–450 G, found for τ_v and Δ in other Mn^{2+} complexes by EPR measurements.[43,44] On the other hand, a similar reasonable fit is obtained if the value chosen for E_v corresponds to a modulation by the rotational diffusion of the complex, i.e., for $E_v = 6$ kcal/mol, which is close to the average of the two E_R values given in Table II. In this case, however, the calculations give τ_v(298 K) = $(5.6 \pm 0.9) \times 10^{-12}$ sec and $\Delta = 408 \pm 32$ G, while a τ_v value of the same order of magnitude as τ_R (see Table II) should be expected if a rotational modulation of a static ZFS interaction really was the dominant mechanism of relaxation for the electrons or at least contributed significantly. It must therefore be concluded that such a mechanism is unimportant, even though the Mn^{2+} ions are in environments that undoubtedly deviate somewhat from cubic symmetry, and the electronic relaxation is primarily caused by molecular collisions. This result is in agreement with the findings of other authors for similar Mn^{2+} complexes with symmetry lower than cubic.[43,45]

When the collision mechanism is dominating, the magnitude of E_v has been found to be in the range of 2.5–4.3 kcal/mol[26,46,47] in the case of aqueous solutions of the $Mn[H_2O]_6^{2+}$ complex, while a value of 1.5 ± 0.1 kcal/mol

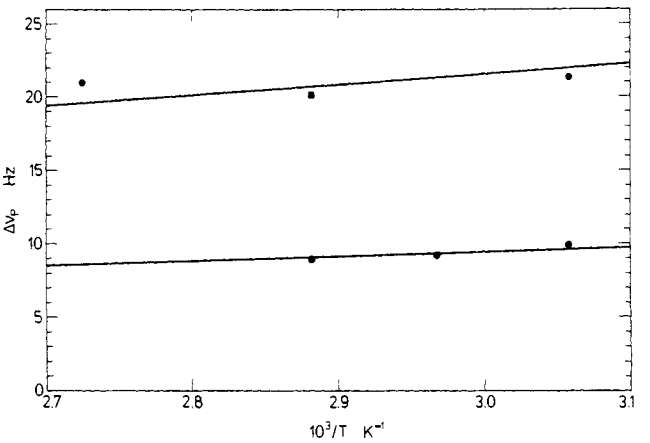

Figure 7. Temperature variation of the isotropic contact shift, $\Delta\nu_P$, for the water protons at 21.1 kG. The experimental values were obtained as described in the text. All shifts are toward lower field. The upper curve is for a 0.01 M solution of the Mn^{2+} ions in water at pH 10.5. The lower curve is for a 1.90 M aqueous solution of histidine identical with the first solution with respect to [Mn^{2+}] and pH.

was obtained for E_v in a study of the Mn^{2+}-pyruvate kinase complex.[48] In the present study E_v can hardly be smaller than 3 kcal/mol since this corresponds to values for Δ and τ_v which are rather unlikely. Thus, for $E_v = 2.7$ kcal/mol the values of Δ and τ_v(298 K) obtained by the fit are 740 G and 1.8×10^{-11} sec, respectively, both of which are incompatible with the above-mentioned EPR results.[43,44] It is therefore reasonable to assume, that the correct value of E_v for the complex studied here is in the range of 3.0–4.5 kcal/mol. Within these limits for E_v, the values of $\Delta H^{\ddagger}$, $\Delta S^{\ddagger}$, τ_M, and τ_v produced by the fit only vary by a little more than their experimental errors, while T_{1e} as well as the rest of the parameters to be determined hardly change at all.

With the obtained parameters the relative importance of the individual relaxation mechanisms discussed in section II can now be evaluated. In Figure 8 is shown the temperature variation of the individual functions $1/\tau_M$, $1/T_{2M}$, and $\Delta\omega_M$ which form part of eq 8. The $1/T_{2M}$ and $\Delta\omega_M$ functions are given for both C(3) and C(5), that is the carbon atom with the smallest and largest $1/T_{2P}$ relaxation rate, respectively. In both cases $\Delta\omega_M^2 \ll (T_{2M}\tau_M)^{-1}$ over the entire experimental temperature range, which reduces eq 8 to:

$$\frac{1}{T_{2P}} = \frac{pq}{(T_{2M} + \tau_M)} \tag{13}$$

As it furthermore appears from Figure 8 $\tau_M \ll T_{2M}$ in the same temperature range for C(3) and in the high-temperature part of the experimental range for C(5). When this inequality holds eq 13 is further reduced to the form $1/T_{2P} = pq/T_{2M}$. For the rest of the carbon atoms the same interpretation applies since, as it appears from Figure 5, the $1/T_{2P}$ curves in these cases are somewhere between the two extremes just discussed. The actual positions depend on the individual A hyperfine coupling constants which, according to eq 2, determine the relative size of the scalar coupling term in $1/T_{2M}$. The bend toward a more positive slope beginning at the high-temperature part of the experimental region, which is observed for all the $(pqT_{2P})^{-1}$ curves in

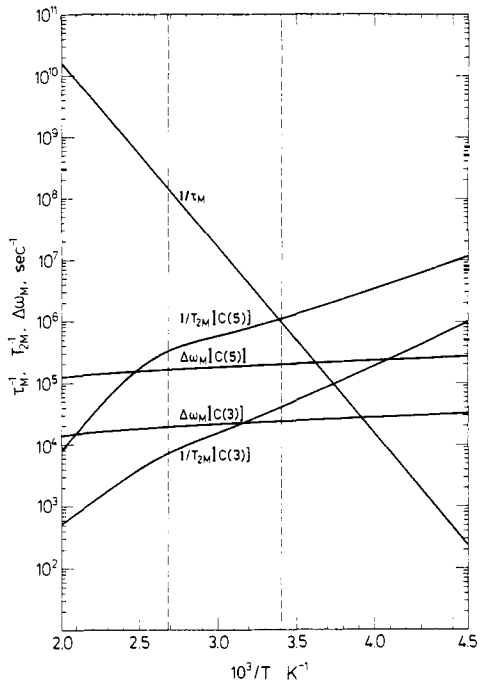

Figure 8. Temperature variation of the spin-spin relaxation rate T_{2M}^{-1} and the isotropic contact shift $\Delta\omega_M$ for C(3) and C(5) at 23.5 kG and the ligand exchange rate τ_M^{-1}, calculated from the parameters in Table II. The dotted lines indicate the experimental temperature region.

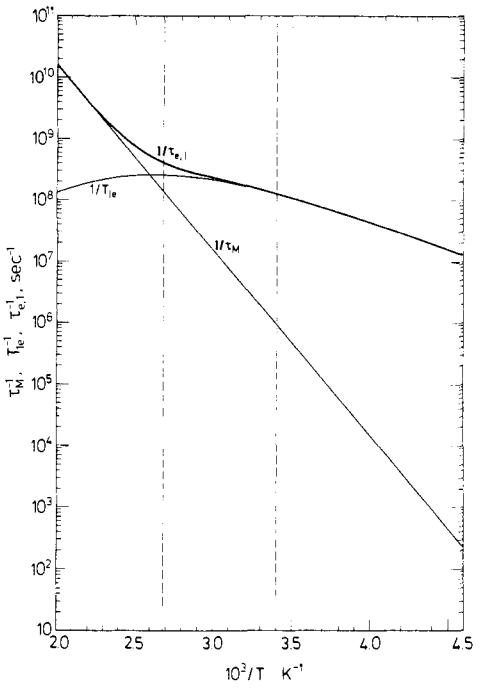

Figure 9. Temperature variation of the electronic spin-lattice relaxation rate T_{1e}^{-1} (see text) at 23.5 kG, the ligand exchange rate τ_M^{-1}, and the sum of these $\tau_{e,1}^{-1}$. The curves were calculated from the parameters in Table II. The dotted lines indicate the experimental temperature region.

Figure 5 and the two $1/T_{2M}$ curves in Figure 8, characterizes the temperature range in which $1/T_{1e}$ is ousted by $1/\tau_M$ from controlling $1/\tau_{e,1}$ and thereby $1/T_{2M}$, according to eq 2. This situation is shown more explicitly in Figure 9. The differences in the slopes of the $(pqT_{2P})^{-1}$ curves in the temperature region above the experimental points reflect the difference in the size of the dipolar term in the $1/T_{2M}$ expressions (eq 2) for the individual carbon atoms. This term is negligible in the experimental temperature region where $1/T_{2M}$ for all six carbons is given by the scalar term in eq 2 alone. At temperatures below the experimental region all $(pqT_{2P})^{-1}$ curves coincide since here $\Delta\omega_M^2$ is the dominant term in eq 8 which reduces all six curves to the form $1/T_{2P} = pq/\tau_M$.

The $\Delta\omega_P$ curves are given by eq 12 in the experimental range except the low-temperature part of the curves for C(4) and C(5). Here $\tau_M \sim T_{2M}$ which invalidates the approximations leading to eq 12 and the curvatures are therefore described by eq 10.

Based on the obtained ligand exchange parameters and the value for pq it is found that $\tau_M \ll pqT_{1P}$ for all T_{1P} values measured here which reduces eq 7 to $1/T_{1P} = pq/T_{1M}$. Also neglect of the scalar coupling term in eq 1 can now be substantiated by inserting the obtained values for the relevant parameters into the Solomon-Bloembergen equation.[20-23] In this evaluation three different T_{2e}'s must be considered, none of which are significantly smaller than T_{1e}.[27] However, even for the hypothetical case with $\tau_{e,2} = 1/\omega_S = 2.42 \times 10^{-12}$ sec which corresponds to the maximum value for the scalar term, it is found that this term in none of the cases contributes more than a few percent of the $(pqT_{1P})^{-1}$ values. Consequently, for all six carbon atoms $1/T_{1M}$ is totally dominated by the electron-nuclear dipolar mechanism. Finally, as pointed out in section II this mechanism should be controlled entirely by the diffusional rotation of the molecules since normally $1/\tau_{e,1} \ll 1/\tau_R$. This assumption is confirmed not only by the found magnitudes of $1/\tau_{e,1}$ and $1/\tau_R$ but also by the fact that the temperature variation of $\tau_{e,1}$ in the experimental range evaluated from Figure 9 is incompatible with the slopes of the curves in Figure 4 given by the temperature dependence of τ_c. This correlation time must therefore be equal to τ_R.

D. Determination of the Structure of the Complex. Based on the conclusions made in the preceding subsection the experimental $1/T_{1P}$ relaxation rates can be written as:

$$\frac{1}{T_{1P}} = \frac{2}{5}\frac{pqS(S+1)g^2\beta^2\gamma_I^2}{r^6}\tau_R \qquad (14)$$

where r and τ_R are the only unknowns. Because of the near-spherical nature of the complex it is assumed that the rotational diffusion causes isotropic tumbling of the molecules in which case a single τ_R can be selected for all six carbons. The significant deviations between the $1/T_{1P}$ values for the various carbons that are found experimentally are therefore attributed to the r^{-6} term alone and eq 14 can be written as:

$$\frac{1}{T_{1P}} = \frac{K}{r^6} \qquad (15)$$

Admittedly, the assumption of an isotropic rotational diffusion tensor is an approximation, as indicated by the small difference between the two E_R values given in Table II, and it may introduce minor errors into the data analysis. Due to the uncertainty in τ_R it is not possible to obtain K in eq 15 to the accuracy required, by calculating it directly from its constituents. On the other hand, K may be evaluated by putting approximate restrains on the structure of the complex. Thus, a distance of 2.22 Å was used for the Mn^{2+}-N bond (see Figure 1) on the basis that the covalent radius of the Mn^{2+} ion is 0.11 Å larger than the covalent radius of the Ni^{2+} ion, which has a 2.09 Å distance to the corresponding nitrogen atom in the bis(histidino)-nickel(II) complex.[49] This number is averaged in with the value of 2.23 Å found for the Mn^{2+}-N bond in the manganese(II)-pyridoxylidenevaline chelate.[50] Furthermore, the Mn^{2+} ion

Table III. Mn^{2+}–C Distances in the Present Histidino–Manganese(II) Complex Calculated from T_1 Relaxation Data, and the Corresponding Ni^{2+}–C Distances in the Bis(histidino)–nickel(II) Complex,[49] Obtained by X-Ray Analysis[a]

	Mn^{2+} complex		Ni^{2+} complex[b]
	310 K	343 K	
r(1), Å	3.01 ± 0.05	3.00 ± 0.05	2.83
r(2), Å	2.93 ± 0.05	2.90 ± 0.05	2.84
r(3), Å	3.49 ± 0.06	3.41 ± 0.05	3.49
r(4), Å	3.19 ± 0.06	3.18 ± 0.06	3.13
r(5), Å	3.24 ± 0.06	3.25 ± 0.06	3.06
r(6), Å	3.65 ± 0.07	3.68 ± 0.07	4.27

[a] The indicated errors are the 2σ confidence limits. [b] The estimated standard deviations of the bond lengths in the Ni^{2+} complex are reported to be 0.01–0.02Å,[49] corresponding to 0.02–0.04Å for the 2σ intervals.

was assumed to be in the plane of the imidazole ring, which has been found with reasonable approximation to be the case for a large number of bivalent metal complexes of histidine and imidazole, without exception.[10] In addition to these restraints on the position of the Mn^{2+} ion, the following structural restraints on the imidazole ring were used[49]: ∠C(4)NC(5) = 107.3°, C(4)–N = 1.329 Å, and C(5)–N = 1.393 Å, where N is the nitrogen atom between C(4) and C(5). The Mn^{2+} ion was then moved about in the plane of the imidazole ring until the $1/T_{1P}$ values for the C(4) and C(5) carbons fit exactly. For the data at 310°C this yields a value of $(6.61 \pm 0.42) \times 10^{-45}$ cm^6/sec for K and $r(4) = (3.19 \pm 0.06)$ Å and $r(5) = (3.24 \pm 0.06)$ Å for the C(4)–Mn^{2+} and the C(5)–Mn^{2+} distances, respectively. For the data at 343 K a similar calculation gave $K = (2.62 \pm 0.20)$ cm^6/sec, $r(4) = (3.18 \pm 0.06)$ Å and $r(5) = (3.25 \pm 0.06)$ Å. From the obtained K values and the experimental $1/T_{1P}$ data the rest of the Mn^{2+}–C distances were calculated using eq 15. All the obtained distances with the estimated 2σ confidence limits are given in Table III together with the corresponding distances for the bis(histidino)–nickel(II) complex taken from the crystal structure.[49] From the two K values the correlation time for the rotational diffusion was estimated to be $\tau_R(310\ K) = (3.83 \pm 0.25) \times 10^{-10}$ sec and $\tau_R(343\ K) = (1.52 \pm 0.12) \times 10^{-10}$ sec, respectively. The activation energy corresponding to this temperature dependence is 5.9 kcal/mol in close agreement with the two E_R values given in Table II.

The excellent agreement between the two sets of Mn^{2+}–C distances exhibited in Table III shows that the same type of Mn^{2+}–histidine complex is formed at both 310 and 343 K. Furthermore, the general accordance between the corresponding manganese and nickel distances indicates strongly that the manganese complex is of the same general nature as found for histidine complexes of other bivalent metal ions in the crystal phase,[10] i.e., a complex where the metal ion is octahedrally coordinated to two nitrogen atoms and an oxygen atom in the histidine ligand, as shown in Figure 1. By comparing the two metal–histidine structures in Table III more closely, it appears that the distances are longer in the manganese complex, except for the Mn^{2+}–C(3) and Mn^{2+}–C(6) distances, which are both shorter than in the nickel complex. However, while Ni^{2+}–C(5) is slightly shorter than Ni^{2+}–C(4), Mn^{2+}–C(5) is longer than Mn^{2+}–C(4), indicating that the imidazole is tipped more toward C(2) in the manganese complex than in the nickel complex. This can be explained by the opening up of the chelate to accommodate the larger covalent radius of the Mn^{2+} ions. As the C(2)–C(3)–C(4) angle will tend to be larger, it is not expected that the Mn^{2+}–C(3) distance will show the same increase. Even a slight decrease of this distance compared to the Ni^{2+}–C(3) distance as indicated by the data is compatible with the model. The increase in the metal–C(2) distance that is slightly smaller than the increase in the covalent radius can also be explained by this effect. On the other hand, the increase in the metal–C(1) distance which is slightly larger than the difference in the covalent radii may indicate a relatively weaker bond for the carboxyl group in the manganese complex. The largest discrepancy between the two structures in Table III is found in the metal–C(6) distances where the value calculated from the relaxation data is significantly smaller than one should expect from the crystal structure of the Ni^{2+}–complex. This discrepancy could in principle result from a nonisotropic tumbling of the complex molecule. More likely, however, it is caused by the delocalization of the paramagnetic electrons, which according to the hyperfine coupling constants in Table II is relatively large at C(6) and could therefore result in a disproportionately short relaxation time for this carbon atom. Also a relative greater importance of the outer sphere relaxation for C(6) could give rise to the discrepancy, especially if a hydrogen bond between the neighboring NH group and the carboxyl group of another ligand histidine molecule, as found for the Ni^{2+}–complex in the crystal phase, is formed. Since none of these effects are incorporated into eq 15 they will show up as errors in the estimate of the metal–ligand distances, and will be most significant for the remote C(6) carbon atom because of the rapid decrease of the efficiency with distance (r^{-6}) of the simple dipolar relaxation mechanism assumed in the derivation of eq 15.

Finally it should be pointed out that the relaxation data only permit a determination of $(r^{-6})_{av}$ that is the average value of r^{-6} over the molecular vibrations, while a calculation of the average distance between Mn^{2+} and a given carbon from eq 15 requires a determination of $(r_{av})^{-6}$, which is different from $(r^{-6})_{av}$. This will, of course, result in an ambiguity in the interpretation of the obtained distances. The good agreement between the obtained structure for the manganese-histidine complex and the X-ray structure of the nickel complex indicates, however, that this ambiguity is irrelevant under the given circumstances, and is probably overshadowed by the experimental uncertainty.

V. Conclusion

The present study demonstrates the feasibility of using T_1 relaxation times of ^{13}C nuclei in a manganese complex to achieve information on the structure in solution. To a relatively high degree of accuracy, the paramagnetic relaxation rate only depends on r^{-6} and not on the angle between the interatomic vector and a coordinate system fixed in the molecule. This makes the method simpler to employ and, therefore, more versatile than structure determination from pseudo-contact shifts caused by lanthanide shift reagents.

This study has also shown that the contribution from the unpaired electrons of the Mn^{2+} ions to the T_2 relaxation of the ^{13}C nuclei is primarily due to a large scalar coupling term which cannot be related to the structure in any simple way.

Acknowledgment. This work was supported in part under Grant RR-574 provided by the Research Resource section of the National Institute of Health. J. J. Led was the recipient of travel grants from the Danish Scientific Research Board and the NATO Science Fellowship Program during a stay at the University of Utah (1971–1973). Part of this work was completed while on leave at the California Institute of Technology as Sherman Fairchild Distinguished Scholar (D.M.G.) and Research Fellow (J.J.L.). We wish to thank Dr. G. O. Sørensen for helpful introduction to his computer program FUNCFIT used in the curve fittings.

Supplementary Material Available. Tables containing the experimental $1/T_1^0$, $1/T_{1,obsd}$, and $1/T_{1P}$ data corresponding to Figure 4 as well as the line width data corresponding to Figure 5 and the chemical shift and contact shift data corresponding to Figure 6 will appear following these pages in the microfilm edition of this volume of the journal. Photocopies of the supplementary material from this paper only or microfiche (105 × 148 mm, 24× reduction, negatives) containing all of the supplementary material for the papers in this issue may be obtained from the Books and Journals Division, American Chemical Society, 1155 16th St., N.W., Washington, D.C. 20036. Remit check or money order for $4.00 for photocopy or $2.50 for microfiche, referring to code number JACS-75-6962.

References and Notes

(1) (a) University of Copenhagen; (b) University of Utah.
(2) (a) A. S. Mildvan and M. Cohn, *Adv. Enzymol. Relat. Areas Mol. Biol.*, **33**, 1 (1970), and references therein; (b) M. Cohn, *Q. Rev. Biophys.*, **3**, 61 (1970).
(3) A. S. Mildvan and J. L. Engle, *Methods Enzymol.*, **26**, 654 (1972).
(4) C. H. Fung, A. S. Mildvan, A. Allerhand, R. Komoroski, and M. C. Scrutton, *Biochemistry*, **12**, 620 (1973).
(5) Y.-F. Lam, G. P. P. Kuntz, and G. Kotowycz, *J. Am. Chem. Soc.*, **96**, 1834 (1974).
(6) A. F. Crockerill, G. L. O. Davies, R. C. Harden, and D. M. Rackham, *Chem. Rev.*, **73**, 553 (1973), and references therein.
(7) C. D. Barry, R. J. P. Williams, and A. V. Xavier, *J. Mol. Biol.*, **84** 471 (1974), and references therein.
(8) A. Abragam, "The Principles of Nuclear Magnetism", Oxford University Press, London, 1961, Chapter VIII.
(9) M. O. Dayhoff, "Atlas of Protein Sequence and Structure", Vol. 5, National Biomedical Research Foundation, Georgetown University Center, 1972.
(10) H. C. Freeman, *Adv. Protein Chem.*, **22**, 257 (1967).
(11) H. Kroll, *J. Am. Chem. Soc.*, **74**, 2034 (1952).
(12) R. H. Carlson and T. L. Brown, *Inorg. Chem.*, **5**, 268 (1966).
(13) I. L. Givot, A. S. Mildvan, and R. H. Abeles, *Fed. Proc., Fed. Am. Soc. Exp. Biol.*, **29**, 531 (1970).
(14) B. R. McGarvey, *Transition Met. Chem.*, **3**, 89 (1966).
(15) M. Tinkham, R. Weinstein, and A. F. Kip, *Phys. Rev.*, **84**, 848 (1951).
(16) R. S. Codrington and N. Bloembergen, *J. Chem. Phys.*, **29**, 600 (1958).
(17) Z. Luz and R. G. Shulman, *J. Chem. Phys.*, **43**, 3750 (1965).
(18) A. R. Peacocke, R. E. Richards, and B. Sheard, *Mol. Phys.*, **16**, 177 (1969).
(19) J. A. McMillan, "Electron Paramagnetism", Reinhold, New York, N.Y., 1968, p 27.
(20) I. Solomon, *Phys. Rev.*, **99**, 559 (1955).
(21) N. Bloembergen, *J. Chem. Phys.*, **27**, 572 (1957).
(22) R. E. Connick and D. Fiat, *J. Chem. Phys.*, **44**, 4103 (1966).
(23) J. Reuben, G. H. Reed, and M. Cohn, *J. Chem. Phys.*, **52**, 1617 (1970).
(24) T. R. Stengle and C. H. Langford, *Coord. Chem. Rev.*, **2**, 349 (1967).
(25) M. Eigen and R. G. Wilkins, *Adv. Chem. Ser.*, **No. 49**, 55, (1965).
(26) N. Bloembergen and L. O. Morgan, *J. Chem. Phys.*, **34**, 842 (1961).
(27) M. Rubinstein, A. Baram, and Z. Luz, *Mol. Phys.*, **20**, 67 (1971).
(28) B. R. McGarvey, *J. Phys. Chem.*, **61**, 1232 (1957).
(29) H. Eyring, *Chem. Rev.*, **17**, 65 (1935).
(30) Z. Luz and S. Meiboom, *J. Chem. Phys.*, **40**, 2686 (1964).
(31) T. J. Swift and R. E. Connick, *J. Chem. Phys.*, **37**, 307 (1962).
(32) N. Bloembergen, *J. Chem. Phys.*, **27**, 595 (1957).
(33) H. M. McConnell and D. B. Chesnut, *J. Chem. Phys.*, **28**, 107 (1958).
(34) R. R. Ernst, *Adv. Magn. Reson.*, **2**, 1 (1966).
(35) D. F. Evans, *J. Chem. Soc.*, 2003 (1959).
(36) J. L. Deutsch and S. M. Poling, *J. Chem. Educ.*, **46**, 167 (1969).
(37) C. C. McDonald and W. D. Phillips, *J. Am. Chem. Soc.*, **85**, 3736 (1963).
(38) E. V. Raju and H. B. Mathur, *J. Inorg. Nucl. Chem.*, **31**, 425 (1969).
(39) R. Hausser and F. Noack, *Z. Phys.*, **182**, 93 (1964).
(40) W. L. Purcell and R. S. Marianelli, *Inorg. Chem.*, **9**, 1724 (1970).
(41) R. H. Henson, D. Phil. Thesis, Oxford 1972.
(42) F. F. Brown, I. D. Campbell, R. H. Henson, C. W. J. Hirst, and R. E. Richards, cited in R. A. Dwek, "Nuclear Magnetic Resonance in Biochemistry", Clarendon Press, Oxford, 1973, p 206.
(43) G. H. Reed, J. S. Leigh, Jr., and J. E. Pearson, *J. Chem. Phys.*, **55**, 3311 (1971).
(44) G. H. Reed and M. Cohn, *J. Biol. Chem.*, **247**, 3073 (1972).
(45) G. H. Reed and M. Cohn, *J. Biol. Chem.*, **245**, 662 (1972).
(46) A. W. Nolle and L. O. Morgan, *J. Chem. Phys.*, **36**, 378 (1962).
(47) C. C. Hinckley and L. O. Morgan, *J. Chem. Phys.*, **44**, 898 (1966).
(48) J. Reuben and M. Cohn, *J. Biol. Chem.*, **245**, 6539 (1970).
(49) K. A. Fraser and M. M. Harding, *J. Chem. Soc. A*, 415 (1967).
(50) E. Willstadter, T. A. Hamor, and J. L. Hoard, *J. Am. Chem. Soc.*, **85**, 1205 (1963).

Ab Initio Calculation Including Electron Correlation of the Structure and Binding Energy of BH_5 and $B_2H_7^-$

Claus Hoheisel and Werner Kutzelnigg*

Contribution from the Lehrstuhl für Theoretische Chemie, Ruhr-Universität Bochum, Bochum-Querenburg, Germany.

Received February 6, 1975

Abstract: Quantum chemical ab initio calculations with and without the inclusion of electron correlation are performed for five possible structures of BH_5 and four possible structures of $B_2H_7^-$. In the SCF approximation BH_5 is not stable with respect to $BH_3 + H_2$; with correlation it has a binding energy of -2 kcal/mol in a C_s geometry. Isomerization is possible via the C_{2v} structure, the energy of which is 9 kcal/mol higher. For $B_2H_7^-$ previous SCF results are confirmed and with correlation the experimental binding energy (with respect to $BH_3 + BH_4^-$) is reproduced. The ion is symmetric with one linear B-H-B bond.

I. Introduction

The molecule BH_5 is isoelectronic to the ion CH_5^+ that has been studied both experimentally[1-3] and theoretically.[4-8] Since CH_5^+ is quite stable as an "ion in space" (its binding energy with respect to $CH_4 + H^+$ is -125 kcal/mol and with respect to $CH_3^+ + H_2$ -40 kcal/mol),[6-8] one could guess that BH_5 should be a stable species as well. Recent experimental studies of the protolysis or hydrolysis[9-11] of BH_4^- led to the postulate of BH_5 as an intermediate in these reactions. A CNDO/2 calculation[9] of four possible structures of BH_5 (belonging to the symmetry groups D_{3h}, C_{3v}, C_{4v}, and C_s) led to the prediction that BH_5 should have C_s symmetry (like CH_5^+) with a binding energy of -1.531 au (~ -40 eV or -900 kcal/mol) with respect to B + 5H. Since this value of the binding energy is rather unrealistic (something similar was observed for other boron hydrides like B_2H_6[12]) the result from the CNDO calculation could not be regarded as definite and we therefore performed a refined ab initio calculation, including electron correlation, with the CEPA-PNO and PNO-CI methods described elsewhere.[14-19]

The ion $B_2H_7^-$ that is well-known from experiment[20-23] is interesting insofar as a structure with a single linear symmetric B-H-B bond has been proposed for this ion. Ab initio studies including correlation of B_2H_6[13,24,25] that has two B-H-B bonds, of $BeBH_5$[26] that is held together by three Be-H-B bonds, and BeB_2H_8[26] where structures with two